Journal of Oceanography, Vol. 65, pp. 439 to 454, 2009

Modeling of the Branches of the Tsushima Warm Current in the Eastern Japan Sea

Hideyuki Kawamura[1]*, Toshimichi Ito[1], Naoki Hirose[2], Tetsutaro Takikawa[3] and Jong-Hwan Yoon[2]

[1]*Research Group for Environmental Science, Nuclear Science and Engineering Directorate, Japan Atomic Energy Agency, Shirakata-shirane, Tokai-mura 319-1195, Japan*
[2]*Center for East Asian Ocean-Atmosphere Research, Research Institute for Applied Mechanics, Kyushu University, Kasuga 816-8580, Japan*
[3]*National Fisheries University, Nagata-honmachi, Shimonoseki 759-6595, Japan*

(Received 11 July 2008; in revised form 19 February 2009; accepted 22 February 2009)

The branches of the Tsushima Warm Current (TWC) are realistically reproduced using a three-dimensional ocean general circulation model (OGCM). Simulated structures of the First Branch and the Second Branch of the TWC (FBTWC and SBTWC) in the eastern Japan Sea are mainly addressed in this study, being compared with measurement in the period September–October 2000. This is the first numerical experiment so far in which the OGCM is laterally exerted by real volume transports measured by acoustic Doppler current profiler (ADCP) through the Tsushima Straits and the Tsugaru Strait. In addition, sea level variation measured by tide-stations along the Japanese coast as well as satellite altimeters is assimilated into the OGCM through a sequential data assimilation method. It is demonstrated that the assimilation of sea level variation at the coastal tide-stations is useful in reproducing oceanic conditions in the nearshore region. We also examine the seasonal variation of the branches of the TWC in the eastern Japan Sea in 2000. It is suggested as a consequence that the FBTWC is continuous along northwestern Honshu Island in summertime, while it degenerates along the coast between the Sado Strait and the Oga Peninsula in other seasons. On the other hand, a mainstream of the SBTWC exists with meanders and eddies in the offshore region deeper than 1000 m to the north of the Sado Island throughout the year.

Keywords:
· Tsushima Warm Current,
· ocean general circulation model,
· ADCP data,
· data assimilation,
· Kalman filter,
· Japan Sea.

1. Introduction

There is a salient difference in the characteristic of circulation in the upper layer (approximately 0–200 m) between the northern part and the southern part of the Japan Sea. Though the circulation in the northern cold region is little known so far, it is believed that the anticlockwise circulation is dominant, with some cyclonic gyres north of the subarctic front (Naganuma, 1977; Yarichin, 1980), which is mainly driven by a northwesterly winter monsoon. In contrast to the northern cold region, the circulation in the southern warm region has been illuminated thanks to relatively abundant observations and numerical experiments (Naganuma, 1977; Yoon, 1982, 1991; Katoh, 1994) and it is known in general that the circulation above the pycnocline is strongly governed by the Tsushima Warm Current (TWC).

The TWC is divided by the Tsushima Islands and it branches into three mainstreams after passing through the Tsushima Straits; one of which flows along the Japanese coast (the First Branch of the TWC (FBTWC) or the Nearshore Branch); the Second Branch of the TWC (hereafter SBTWC) flows off the FBTWC and the other one flows northward along the Korean coast as the East Korean Warm Current (EKWC). The numerical experiments (Yoon, 1982, 1991) suggest that the FBTWC is controlled by bottom topography in the shelf region shallower than 200 m along the Japanese coast, while the EKWC is formed by the planetary β effect with seasonally varying flow pattern. With regard to the SBTWC, an analysis of temperature distribution at 100 m depth during the pe-

* Corresponding author. E-mail: kawamura.hideyuki@jaea.go.jp

riod from 1963 to 1989 (Hase *et al*., 1999) allows us to conclude that it is topographically steered and develops along the continental shelf break west of the Noto Peninsula from spring to fall. According to Nakada *et al*. (2002), the SBTWC experiences transformation from barotropic flow to baroclinic flow near the Noto Peninsula and thereafter separates from the continental shelf break as the offshore front in the eastern Japan Sea.

Although the TWC is very complicated and it has large variability in the Japan Sea, it is fundamentally driven by the sea level difference between the East China Sea and the region east of the Tsugaru Strait in the Pacific Ocean (Toba *et al*., 1982). According to an intensive survey of mechanism of the TWC, using an analytical model and ocean general circulation model (OGCM), wind stress forcing over the North Pacific is mainly responsible for the formation and seasonal variation of the TWC through an adjustment process involving baroclinic Rossby waves and coastally trapped waves (Tsujino *et al*., 2008).

Taking past observation and numerical research into account, a numerical experiment on the TWC must incorporate exact volume transports through the straits connecting the Japan Sea and open oceans. Long-term, multilevel acoustic Doppler current profiler (ADCP) observation has recently been conducted by a ferryboat, the "*Camellia*", through the Tsushima Straits since February 1997. It was reported that the total volume transport averaged over the observational period (5.5 years) is 2.64 Sv (Sv $\equiv 10^6$ m^3/s) with 1.10 Sv across the eastern channel and 1.54 Sv across the western channel, respectively (Takikawa *et al*., 2005). Moreover, ADCP observation by the ferryboat "*M.V. Virgo*" has been carried out through the Tsugaru Strait during November 1999–December 2007. Ito *et al*. (2003) reported that the volume transport of the Tsugaru Warm Current varies from 1.1 to 2.5 Sv with a mean value of 1.5 Sv in the period November 1999–March 2000.

In this study, the numerical experiment is performed using the three-dimensional OGCM. The OGCM is laterally forced by the daily mean volume transports in 2000 estimated from ADCP measurement, as explained above, through the Tsushima Straits and the Tsugaru Strait. A data assimilation experiment is further carried out to improve the deficiency of the numerical model. According to Hirose *et al*. (2007), who surveyed the in-depth quantitative analyses of data assimilation, the subsurface condition associated with mesoscale eddies is improved, especially in the southern part of the Japan Sea by assimilating sea surface height and sea surface temperature provided by satellite data into the OGCM. In one of our numerical experiments, not only satellite altimeter data but also sea level data obtained at 19 tide-stations along the Japanese coast (Fig. 1) are assimilated into the OGCM,

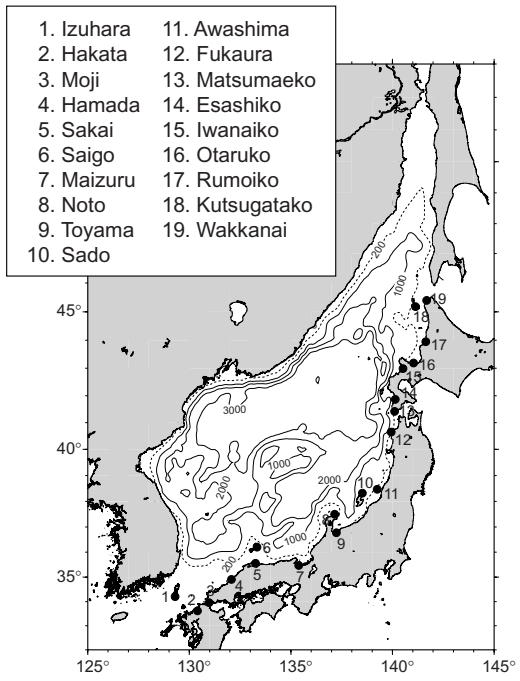

Fig. 1. Bottom topography in the Japan Sea with contour interval (C.I.) = 1000 m. Dashed line denotes the 200 m isobath. Numbers show the coastal tide-stations in which sea level data from the Japan Oceanographic Data Center (JODC) are used for the data assimilation experiment.

which we expect that the oceanic condition in the nearshore region will modify.

This study aims to reproduce the branches of the TWC making use of the ADCP data measured across the Tsushima Straits and the Tsugaru Strait and assimilating sea level variation obtained by satellites and coastal tide-stations. Our interest is mainly confined to the eastern Japan Sea and model results are therefore compared with observational results in the eastern Japan Sea in the period September–October 2000 (Watanabe *et al*., 2006). Moreover, the seasonal variation of the branches of the TWC in 2000 is briefly examined in light of the model results.

This paper is organized as follows. Configurations of the OGCM are described in Subsection 2.1 and data assimilation schemes are explained in Subsection 2.2. Section 3 gives the results of the numerical experiments. Finally, Conclusions are presented in Section 4.

2. Numerical Experiment

2.1 Hydrodynamic model

The three-dimensional OGCM used in this study is the Research Institute for Applied Mechanics Ocean Model (RIAMOM) (Lee, 1996; Lee *et al*., 2003), which

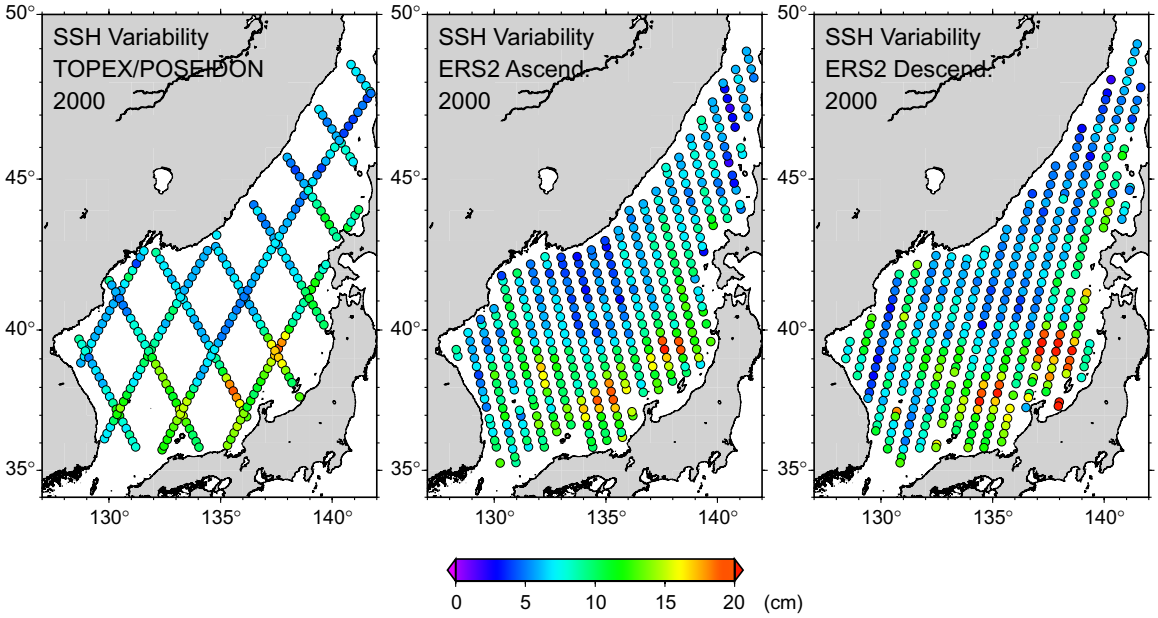

Fig. 2. Standard deviation (cm) of the sea surface height obtained from the TOPEX/POSEIDON, ascending and descending path of the ERS2. Data are subsampled at one day intervals. Satellite ERS2 traveled westward opposite to the TOPEX/POSEIDON and the northwestward track is the ascending path, while the southwestward track is the descending path.

is still undergoing further refinement at Kyushu University. This is a multi-level primitive equation model with mode splitting (Blumberg and Mellor, 1987) under the Boussinesq approximation and the hydrostatic assumption on spherical coordinates in horizontal and the z-coordinate in vertical. Longer time steps with 20 seconds for the external mode and 480 seconds for the internal mode, respectively, are permitted by adopting a Shuman filter (Shuman, 1957). The model domain is identical to that of Hirose *et al*. (2007) covering the entire Japan Sea (Fig. 1). Horizontal grid resolutions are chosen as 1/12° in both latitude and longitude with 36 variable levels in the deepest bottom and partial stepping for bottom cell is vertically allowed (Adcroft *et al*., 1997).

Coefficients of horizontal and vertical eddy viscosity are set to 1.0×10^6 and 1.0 cm^2/s, respectively. Tracer mixing is parameterized by the turbulent closure model (Noh and Kim, 1999) and the isopycnal diffusion scheme (Gent and McWilliams, 1990). Tracer advection is implemented by the high-order modified split quadratic upstream interpolation for a convective kinematics scheme (Webb *et al*., 1998), with which the slant advection scheme is incorporated in order to avoid the diffusive current on the shelf break. For details of the RIAMOM, readers are referred to Lee (1996).

Twice-daily wind stress applied at the sea surface is given by the output in 2000 of the mesoscale atmospheric model from the Japan Meteorological Agency (JMA). The no-flux boundary condition is used at the sea bottom for temperature and salinity, while thermohaline forcing is applied at the sea surface. The imposed heat and salt flux at the sea surface are given by the so-called Newtonian type restoring boundary condition with damping time scales of 5 and 10 days for temperature and salinity, respectively. The temperature in the first level is restored to the monthly mean sea surface temperature in 2000 calculated using the high-resolution (0.01° in both latitude and longitude) data of satellite from Tohoku University (Sakaida *et al*., 2000). The long-term monthly mean sea surface salinity is issued for salt flux using data files of the Japan Oceanographic Data Center (JODC), Fisheries Research and Development Agency of Korea (FRDAK) and Far Eastern Regional Hydrometeorological Research Institute (FERHRI) of Russia.

We use the ADCP data in 2000 obtained by the ferryboats as the lateral boundary conditions of inflow volume transport through the Tsushima Straits (Takikawa *et al*., 2005) and outflow volume transport through the Tsugaru Strait (Ito *et al*., 2003). At the inflow region, the total throughflow transport is given, divided into two components through the eastern channel and the western channel. The rest of the volume transport passes out through the Soya Strait. The Mamiya Strait is closed owing mainly to its smallness to throughflow transport. The inlet internal component of current at the inflow region is diagnosed from the prescribed temperature and salinity distribution along the boundaries, based on the assumption of thermal wind relation. The internal struc-

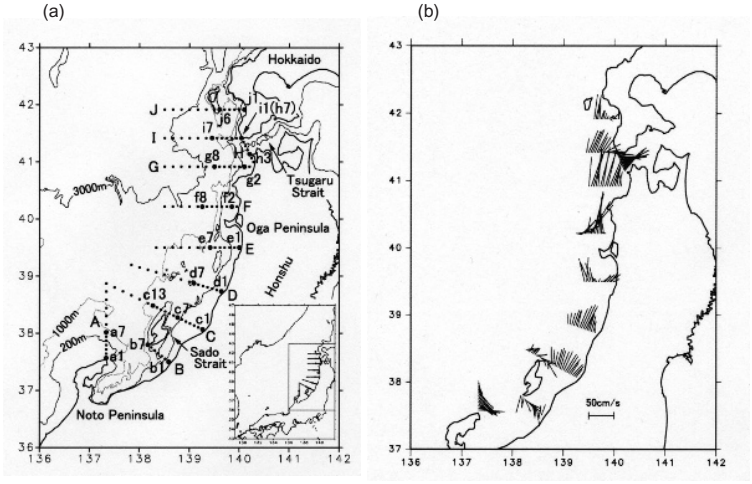

Fig. 3. Area of observation campaign conducted in the period September–October 2000 in the eastern Japan Sea, reprinted with permission from figure 1 in Watanabe *et al*. (2006), Copyright (2006) Oceanographic Society of Japan (a), and observed distribution of the daily mean current across the ADCP lines at the depth of 38 m reprinted with permission from figure 4 in Watanabe *et al*. (2006), Copyright (2006) Oceanographic Society of Japan (b). Capital letters and small letters with numbers indicate names of the ADCP lines and the CTD stations, respectively.

tures of current are set as same as those at adjacent interior points and no normal gradient conditions are applied for temperature and salinity at the Tsugaru Strait and the Soya Strait.

The time integration is carried out from a static state for 20 years as the spin-up period in advance. During the spin-up period, the numerical model is nudged by the reanalyzed monthly mean wind stress provided by the European Centre for Medium-Range Weather Forecasts (ECMWF) and the heat flux at the sea surface is specified by the Haney type heat flux (Haney, 1971). After the spin-up period, three experiments are performed: one is forward modeling with no data assimilation (hereafter referred to as EXP1). Experiment EXP2 is carried out by assimilating the along-track altimeter data of the TOPEX/POSEIDON and the ERS2 (Fig. 2) into the numerical model. The experiment assimilating sea level variation obtained by the coastal tide-stations along the Japanese coast as well as the satellite altimeters is here referred to as EXP3.

2.2 Data assimilation

The data assimilation is a dynamical and statistical combination of measurement data and numerical model. The sequential data assimilation of sea level variation into the eddy-resolving OGCM in experiments EXP2 and EXP3 is conducted by means of a Kalman filter (Fukumori and Malanotte-Rizzoli, 1995; Hirose *et al*., 2007), which is one of the major optimal and feasible algorithms. The sea surface topography reflects the integral effect of the ocean interior and we accordingly expect a subsurface correction by solving an inverse problem so as to satisfy the measurement data as well as the physics in the numerical model.

A model state vector x is updated in time (t) by the measurement data at each following instant as,

$$x(t) = x(t,-) + K(t)\left[z(t) - H(t)x(t,-)\right]. \quad (1)$$

Here z denotes the measurement data and H is an observation operator that maps the model state to observational point. A minus sign indicates a prediction stage before updating by the measurement data, while no minus sign means a filtered stage after updating. The Kalman gain matrix K essentially plays the role of weighting between the observation and the numerical model, which is calculated as:

$$K(t) = P(t,-)H^T(t)\left[H(t)P(t,-)H^T(t) + R(t)\right]^{-1}. \quad (2)$$

The matrices P and R indicate the system error covariance matrix and the data error covariance matrix. In the equation the superscripts T and -1 denote matrix transpose and inversion, respectively. The data error covariance matrix is preliminarily constructed by matching the covariance of measurement data and model results in the absence of data assimilation, according to Fu *et al*. (1993). On the other hand, the system error covariance matrix is dynamically updated in time by the Lyapunov equation as follows:

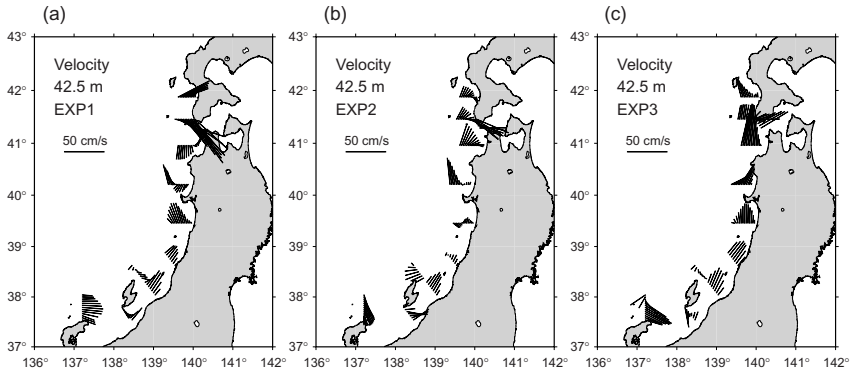

Fig. 4. Distribution of the mean current across the ADCP lines at a depth of 42.5 m in experiments EXP1 (a), EXP2 (b) and EXP3 (c).

Table 1. Mean volume transports in Sv normal to the ADCP lines. The eastward, northeastward or northward direction is positive.

ADCP line	A	B	C1	C2	D	E	F	G	H	I	J
Both ends	a1–a7	b1–b7	c1–c7	c7–c13	d1–d7	e1–e7	f2–f8	g2–g8	h3–h7	i1–i7	j1–j6
Period	Sep. 18–19	Sep. 16–17	Sep. 25–26	Sep. 22–23	Sep. 27–28	Sep. 29–30	Oct. 1–2	Oct. 3–4	Oct. 5–6	Oct. 6–7	Oct. 8–9
Mean transport (Sv)											
Observation*	1.34	−0.26	1.09	0.08	1.08	0.44	1.61	1.92	1.53	0.90	0.46
EXP1	1.47	0.07	0.48	−0.07	−0.01	0.42	−0.25	−1.82	0.52	−2.34	0.68
EXP2	0.93	0.47	0.40	−0.28	−0.14	−0.12	0.64	0.11	0.70	−0.13	−0.12
EXP3	1.37	−0.18	0.61	−0.20	0.63	0.45	0.54	1.99	0.85	0.95	0.67

*Watanabe *et al*. (2006).

$$P(t+1,-) = AP(t)A^T + \Gamma Q \Gamma^T, \tag{3}$$

where A and $\Gamma Q \Gamma^T$ are the state transition matrix and the process noise. The magnitude of the system error covariance matrix is reduced by measurement update as:

$$P(t) = P(t,-) - K(t)H(t)P(t,-). \tag{4}$$

The model state vector is separated into the barotropic and the baroclinic mode in this study. The barotropic state vector consists of the barotropic component of velocity and sea surface height. On the other hand, the baroclinic state vector is composed of interface and amplitude of the first baroclinic mode and the second baroclinic mode, which are estimated from the eigenvalue decomposition (Gill, 1982) to reduce computational burden. Although Hirose *et al*. (2007) extracted only the first baroclinic mode, the second baroclinic mode must be significant to reproduce the density structure along the Japanese coast, because it is prominent in the nearshore region of subsurface countercurrent beneath the TWC (Sasajima *et al*., 2007). For more details of the data assimilation used in this study, readers are referred to Hirose (1999).

3. Results

3.1 Effect of data assimilation on current structure

Watanabe *et al*. (2006) conducted the ADCP measurement with a four round-trip method in order to remove the diurnal and semidiurnal tidal current and the CTD measurement along lines A–J (Fig. 3(a)) in the eastern Japan Sea in the period September–October 2000. They examined the current structure and the volume transport of the TWC along the northwestern Japanese coast. Figure 3(b) displays the observed distribution of diurnally-averaged current across the ADCP lines at 38 m depth, in which the eastward, northeastward or northward current regarded as the TWC clearly exists along the northwestern Japanese coast, except for line B at an entrance to the Sado Strait. The current field at 42.5 m depth along the

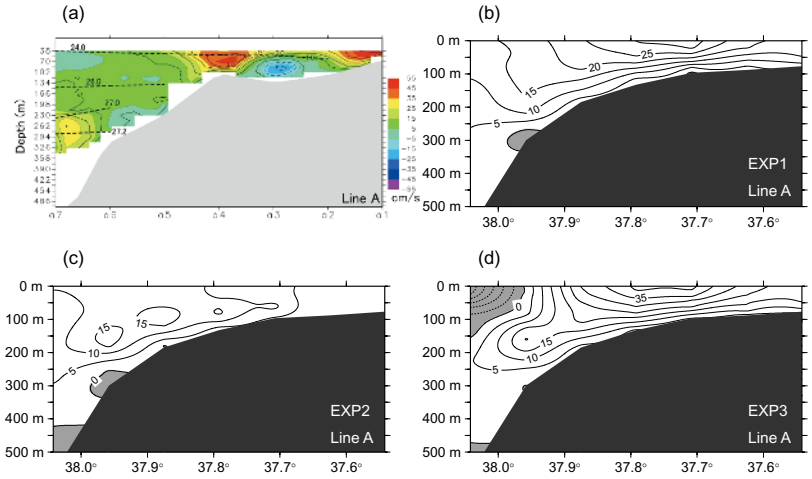

Fig. 5. Observed daily mean current normal to ADCP line A (a) reprinted with permission from figure 3 in Watanabe *et al*. (2006), Copyright (2006) Oceanographic Society of Japan, where the dashed line indicates the potential density (σ_θ). Mean current with C.I. = 5 cm/s in experiments EXP1 (b), EXP2 (c) and EXP3 (d) normal to ADCP line A. Shaded area denotes westward current.

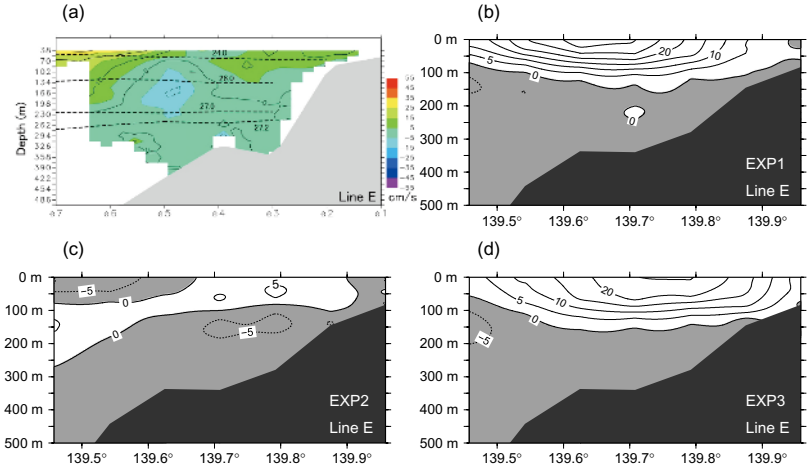

Fig. 6. As Fig. 5 except along ADCP line E. Shaded area denotes the southward current.

ADCP lines is shown in Fig. 4(a), averaged in each observational period (Table 1) in experiment EXP1. Though the model result is in fairly good agreement with the observational result south of the Oga Peninsula, the correlation in the northern region, such as lines G, H and I, is relatively poor. Among other problems, the southward current on the east side of line F and across lines G and I is found with a direction opposite to the observed northward current. This disagreement may be attributed to the existence of an anti-cyclonic eddy generated to the west of the Tsugaru Strait, which is not seen in Fig. 3(b).

Observed transects of the diurnally-averaged current normal to lines A, E, F, G and I are presented in Figs. 5(a)–9(a), where the white area indicates missing or unreliable data. Corresponding vertical sections in experiment EXP1 are also shown in Figs. 5(b)–9(b), where the westward or southward subsurface countercurrent is produced on the bottom of the continental shelf at all lines. Although the subsurface countercurrent south of the Oga Peninsula (lines A and E) is roughly comparable with the observed current, it is quite strong along the northern lines (lines F, G and I), which may be affected by the clockwise eddy to the west of the Tsugaru Strait.

Similar to the current distribution, there is a discrepancy between the measured data and the model result in the sea level variation along the Japanese coast. The diurnally-averaged sea level anomalies from annual mean at Sakai, Maizuru, Toyama, Awashima, Fukaura and

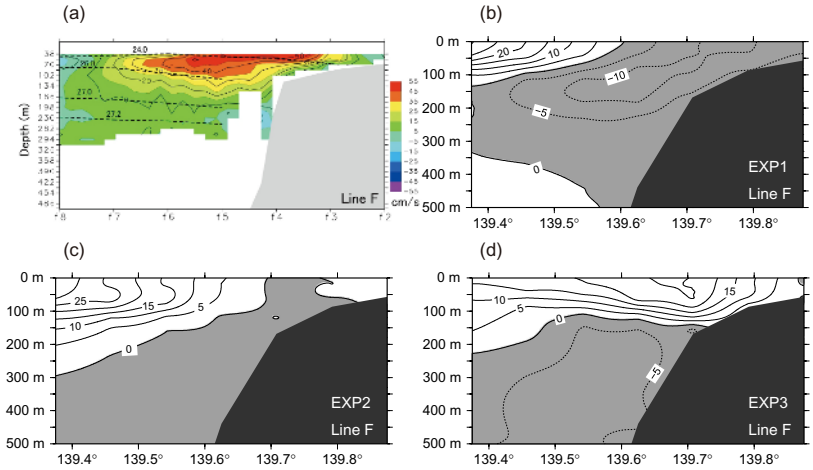

Fig. 7. As Fig. 6 except along ADCP line F.

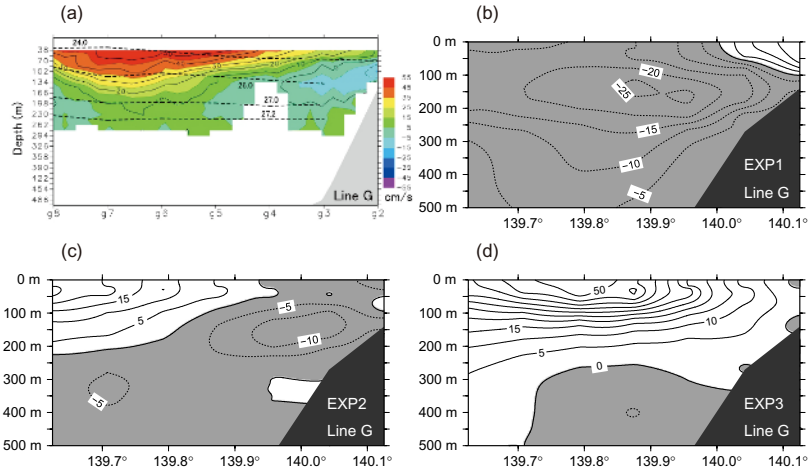

Fig. 8. As Fig. 6 except along ADCP line G.

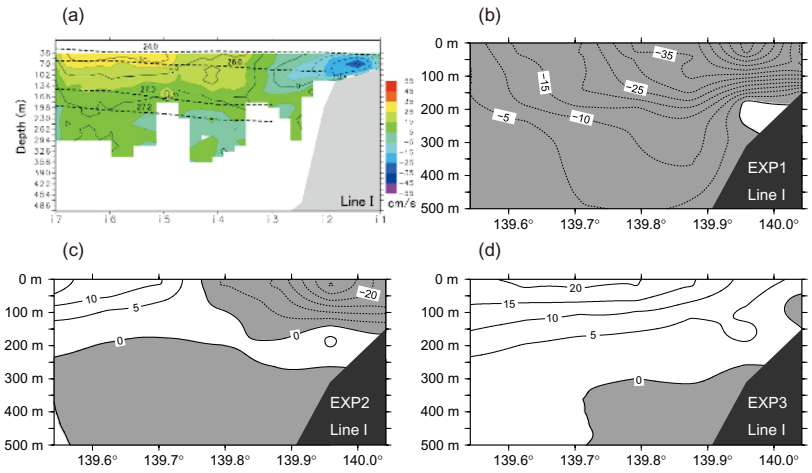

Fig. 9. As Fig. 6 except along ADCP line I.

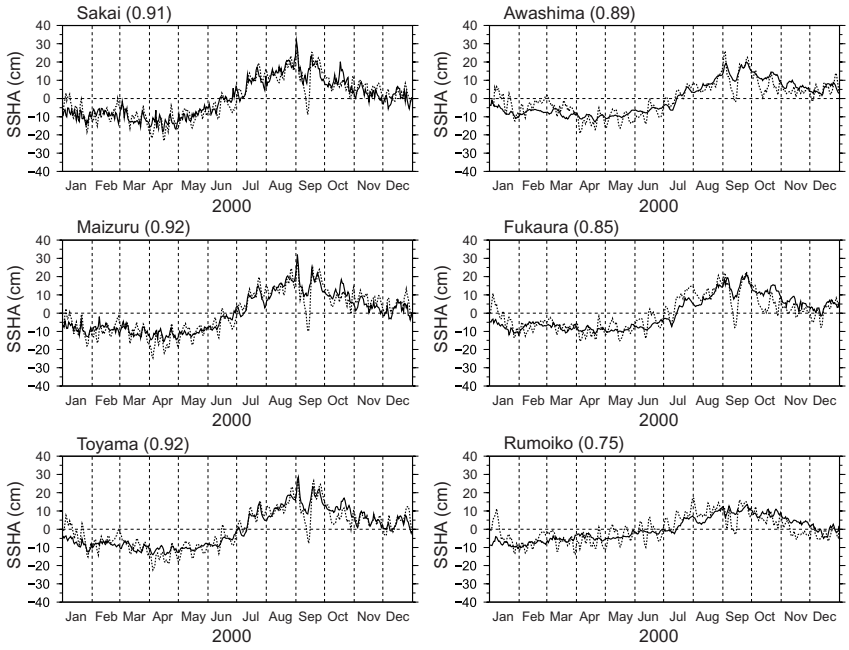

Fig. 10. Observed sea level anomaly (dashed line) and sea level anomaly in experiment EXP1 (solid line) in cm at the coastal tide-stations Sakai, Maizuru, Toyama, Awashima, Fukaura and Rumoiko. Numbers in parentheses denote the correlation coefficients.

Rumoiko in experiment EXP1 are shown by solid lines in Fig. 10. The seasonal sea level variation is readily found with the maximum in summer and the minimum in winter, and the amplitudes in the southern Japan Sea (Sakai, Maizuru and Toyama) are larger than those in the northern Japan Sea (Awashima, Fukaura and Rumoiko). The difference in the amplitude of sea level variation between the southern region and the northern region is also identified by the standard deviation of sea level measured by the satellite altimeters of the TOPEX/POSEIDON and the ERS2 (Fig. 2). This seasonal variation must be mainly caused by the throughflow transports across the Tsushima Straits and the steric height, which is simply calculated under mass conservation in the RIAMOM. Although a fairly good relationship is obtained with correlation coefficients of 0.91, 0.92 and 0.92 against the observed sea level variation shown by dashed lines in Fig. 10 at Sakai, Maizuru and Toyama, the correlation becomes worse in the northern region, such as Awashima, Fukaura and Rumoiko. In particular, the high frequency variation with a period of a few weeks is not realistically reproduced in the northern Japan Sea; on the other hand it must be due to the daily mean inflow boundary condition at the Tsushima Straits upstream of the TWC that short-period sea level oscillation in the southern region is relatively well reproduced.

The sea level variation along the Japanese coast must be closely related to the behavior of the TWC, as suggested by Ishikawa *et al*. (2007). Figure 11 shows the relationship between the diurnally-averaged sea level variation observed at the coastal tide-station Maizuru (Fig. 1) possibly located on a downstream section of the FBTWC and the diurnally-averaged volume transports through the Tsushima Straits (Fig. 11(a)) and the Tsugaru Strait (Fig. 11(b)) in 2000. The volume transport across the Tsugaru Strait is not drawn for about the first three months when only the data smoothed by the 15-day running mean filter were obtained. As for the sea level variation, the effect associated with tide and atmospheric pressure is almost removed. The values of volume transports and sea level are anomalies, subtracting their annual mean values. The volume transport through the Tsushima Straits varies seasonally with a maximum in summer (July–September) and a minimum in winter (January–March) in 2000, although its seasonal variation at the Tsugaru Strait is relatively obscure. A similar seasonal variation is apparently found in a sea level record at the coastal tide-station Maizuru, which attains a maximum in September and a minimum in April. The high-frequency variation with the period of a few weeks as well as the seasonal variation of sea level anomaly is in agreement with the short-period variation of throughflow transports across the two straits. It is particularly remarkable that the volume transport across the Tsushima Straits decreases considerably by about 3.5 Sv in September, which may be caused by typhoon No. 14 passing the Tsushima Straits

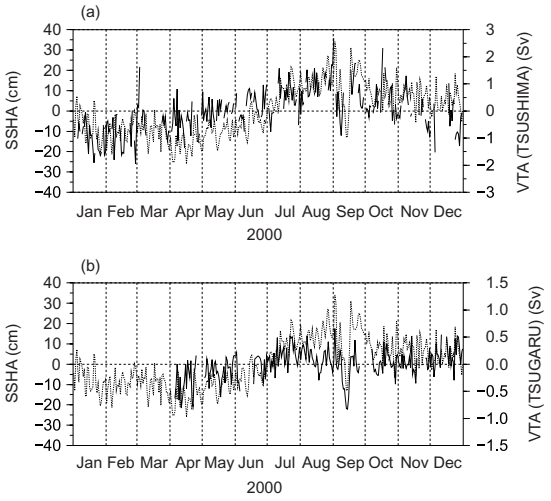

Fig. 11. Observed sea level anomaly in cm represented as dashed line at the coastal tide-station Maizuru and volume transport anomaly in Sv as solid line through the Tsushima Straits (a) and the Tsugaru Strait (b), respectively.

toward the north, when the sea level at Maizuru falls and the volume transport across the Tsugaru Strait declines by about 1.5 Sv. The above confirms that the sea level variation along the Japanese coast must be strongly correlated with the volume transports through the Tsushima Straits and the Tsugaru Strait. The ADCP measurement data used as the inflow boundary condition is beneficial in that the sea level variation is well reproduced in the southern Japan Sea in experiment EXP1. However, the TWC becomes more complicated east of Noto Peninsula, since the shelf in the pathway of the coastal branch flow of the TWC breaks at Toyama Bay, and this may be one reason why the current distribution and sea level variation are not realistically reproduced in the nearshore region of the northern Japan Sea in experiment EXP1. Therefore the Kalman filter, one of the data assimilation schemes, is applied to the OGCM to resolve these problems.

Data assimilation experiments EXP2 and EXP3 are performed with the satellite altimeter data and the sea level data at the tide-stations along the Japanese coast. The along-track satellite altimeter data of the TOPEX/POSEIDON and the ERS2 is sequentially assimilated into the OGCM in experiment EXP2, while the sea level data obtained at 19 tide-stations along the Japanese coast as well as the satellite altimeter data are used for the data assimilation in experiment EXP3. The current distribution at a depth of 42.5 m is shown in Figs. 4(b) and (c) in experiments EXP2 and EXP3, respectively. Although the southward current on the east side of line F and across lines G, H and I in experiment EXP1 is modified to the northward current, similarly to the observed current, the coastal current between the Sado Strait and the Oga Peninsula is obscure compared with the observed strong current in experiment EXP2 (Fig. 4(b)). The satellite altimeter data in the nearshore region shallower than 200 m is in general eliminated (Fig. 2) because of inaccuracy such as the tidal correction, and the assimilation of only satellite altimeter data may accordingly be insufficient to improve the oceanic condition in the coastal area. On the other hand, the current distribution at the depth of 42.5 m in experiment EXP3 gives the best agreement with the observed current of the three numerical experiments, although the magnitude of velocity is relatively weak (Fig. 4(c)). The eastward, northeastward or northward current along the northwestern Japanese coast is obviously continuous and furthermore the southward current across line B at the mouth of the Sado Strait is also reproduced. The horizontal grid resolution of 1/12° (about 9 km) in the numerical model is able to resolve perturbations associated with the mesoscale eddy in the ocean interior, which must be insufficient for modeling in the coastal area. As mentioned above, the sea level variation in the southern Japan Sea is well reproduced thanks to the ADCP data through the Tsushima Straits in experiment EXP1 (Fig. 10). However, the downstream current structure or wave propagation, such as Kelvin waves near the coast, gradually becomes inaccurate due to a lack of horizontal grid resolution. In experiment EXP3, the coastal current must be modified, especially in the northern Japan Sea through quasi-geostrophic adjustment by sea level difference between the satellite altimeters and the coastal tide-stations.

The transects of the mean current across ADCP lines A, E, F, G and I are shown as Figs. 5(c)–9(c) in experiment EXP2 and as Figs. 5(d)–9(d) in experiment EXP3. As mentioned in Subsection 2.2, the subsurface correction by means of the assimilation of sea surface topography is expected in experiments EXP2 and EXP3. Although the vertical structure of normal velocity is apparently modified along lines F, G and I in experiment EXP2, no improvement is evident south of the Oga Peninsula. As for experiment EXP3, the vertical current structure across the ADCP lines is realistically reproduced on the whole. For instance, the eastward or northward strong current with axis speed over 40 cm/s at line A, 25 cm/s at line F, 50 cm/s at line G and 20 cm/s at line I is found at the sea surface and the location of cores is in agreement with the observed surface current. Although it is difficult to compare with the observational results below about 300 m, since many data are missing or unreliable, the results of experiment EXP3 suggest that the subsurface countercurrent is generated along the eastern Japanese coast as well as the western Japanese coast in this season, accompanied by clockwise eddies (see the current distribution at 302.5 m depth in Fig. 12(b)). The subsurface countercur-

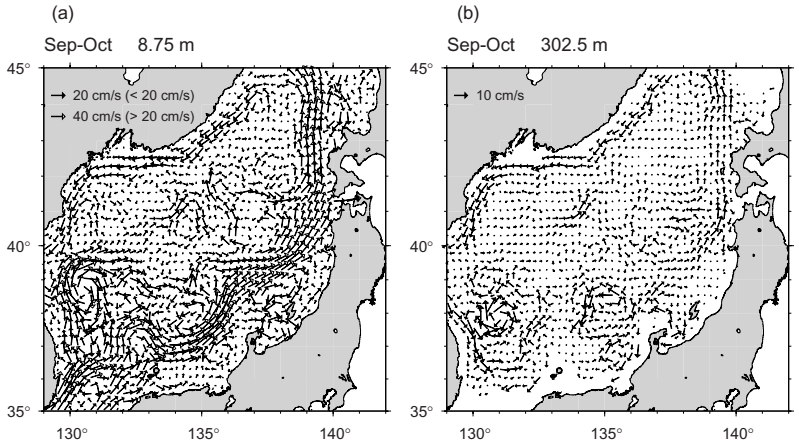

Fig. 12. Horizontal distribution of the mean current at depths of 8.75 (a) and 302.5 (b) m during September and October in experiment EXP3.

rent has actually been reported along the southwestern Honshu Island (Katoh *et al*., 1996: Hase *et al*., 1999). The subsurface countercurrent in the nearshore region from spring to early winter was also found to appear in the numerical experiment by Sasajima *et al*. (2007), who suggested that the second baroclinic mode is responsible for the subsurface countercurrent beneath the TWC in the nearshore region.

Watanabe *et al*. (2006) estimated the volume transports across lines A–J as presented in Table 1, where a positive value means eastward, northeastward or northward volume transport. Because the data are very scarce or unreliable in the near surface layer and the deeper layer below about 300 m depth, as shown in Figs. 5(a)–9(a), they extrapolated the velocity of the first layer at 38 m depth for the near surface layer from the sea surface to 30 m depth and the velocity in the deeper layer below about 300 m depth was omitted when calculating the volume transports. The volume transports are also listed in Table 1 between sea surface and 290 m depth across the ADCP lines, as estimated in the numerical experiments. Although an exact comparison is quantitatively difficult due to the absence or unreliability of data in the observational results, the volume transports in experiment EXP3 give the best agreement with their estimates. In the observational results, the volume transports increase drastically at lines F (1.61 Sv) and G (1.92 Sv) from line E (0.44 Sv), suggesting that the offshore SBTWC and the eastward current established by the subarctic front are combined with the coastal FBTWC to the north of the Oga Peninsula. It is supposed that the same phenomenon is reproduced in experiment EXP3, although the volume transport across line F is small compared with the observed value. Moreover, this phenomenon is demonstrated by the mainstream of the SBTWC in the mean current

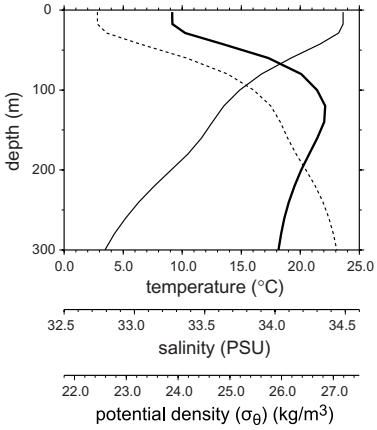

Fig. 13. Vertical profile of temperature (°C) (thin line), salinity (PSU) (thick line) and potential density (σ_θ) (kg/m^3) (dashed line) at station f6 between stations f2 and f8 in Fig. 3(a) in experiment EXP3.

distribution at a depth of 8.75 m during September and October in 2000 (Fig. 12(a)). Figure 12(a) also suggests that the southwestward volume transport across line B may stem from the clockwise eddy southwest of Sado Island, which persists for a few months, although Watanabe *et al*. (2006) speculated that it is due to the local temporal wind condition.

The data assimilation of sea level variation measured by the satellite altimeters must be effective in modifying the oceanic condition in the ocean interior, but it may, however, be insufficient for the nearshore region on account of the inaccuracy of satellite altimeter data in the shallow region. As discussed above, it is verified that the sequential data assimilation of sea level variation at the

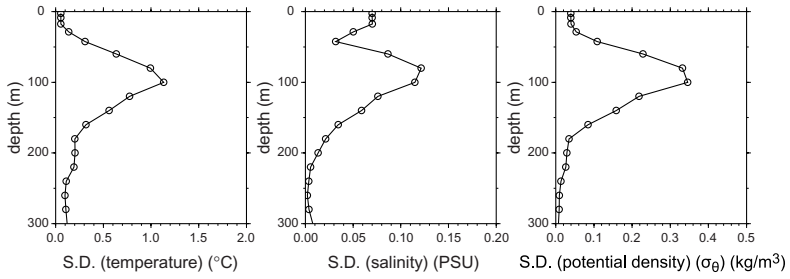

Fig. 14. Standard deviation from the horizontally-averaged value of temperature (°C), salinity (PSU) and potential density (σ_θ) (kg/m^3) at ADCP line F in experiment EXP3.

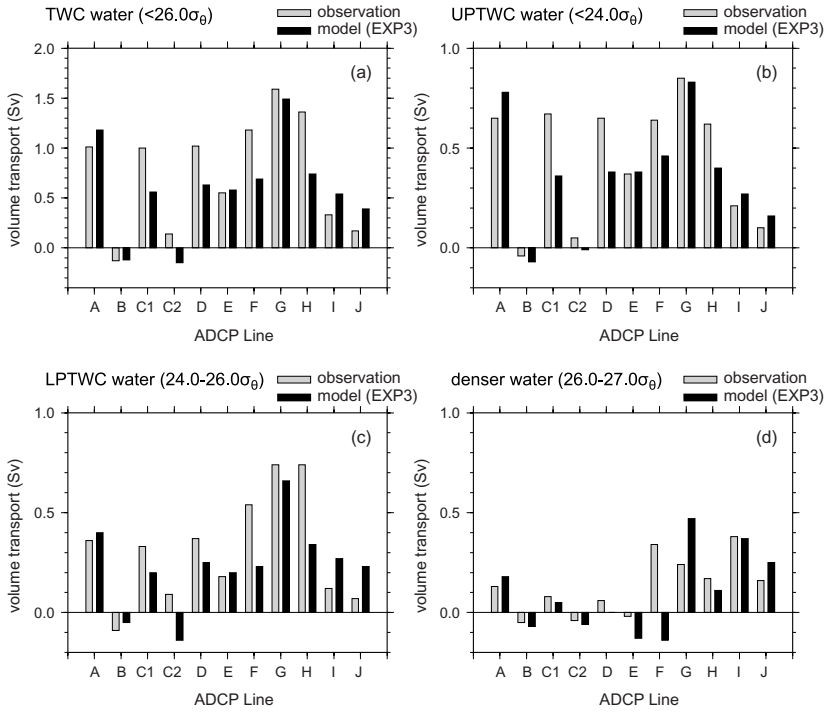

Fig. 15. Mean volume transports across the ADCP lines in each observational period in Sv estimated by observation (Watanabe *et al*., 2006) and experiment EXP3. Volume transports are divided by the potential density (σ_θ) range corresponding to the TWC water (<26.0σ_θ) (a), the UPTWC water (<24.0σ_θ) (b), the LPTWC water (24.0–26.0σ_θ) (c) and the denser water (26.0–27.0σ_θ) (d).

tide-stations along the Japanese coast plays a significant part in reproducing the oceanic field in the coastal region. In the subsequent Subsections 3.2 and 3.3, the analyses are performed making use of the results in experiment EXP3 to examine the TWC.

3.2 Upper and lower portion of the TWC

The vertical profiles of temperature, salinity and potential density (σ_θ) in experiment EXP3 are shown in Fig. 13 at station f6 between stations f2 and f8 (Fig. 3(a)) in the northeastern Japan Sea. The profile is in agreement with the observed profile (figure 7 in Watanabe *et al*., 2006), although a more diffusive thermocline and halocline are formed than noted in the observational results, and the subsurface salinity maximum occurs in a slightly deeper layer, one reason being the inherent numerical diffusion. From an analysis of standard deviation from the horizontally-averaged values along line F, the largest standard deviation of temperature, salinity and potential density is found at a depth of about 100 m, corresponding to the subsurface salinity maximum layer (Fig. 14). The subsurface salinity maximum is obviously

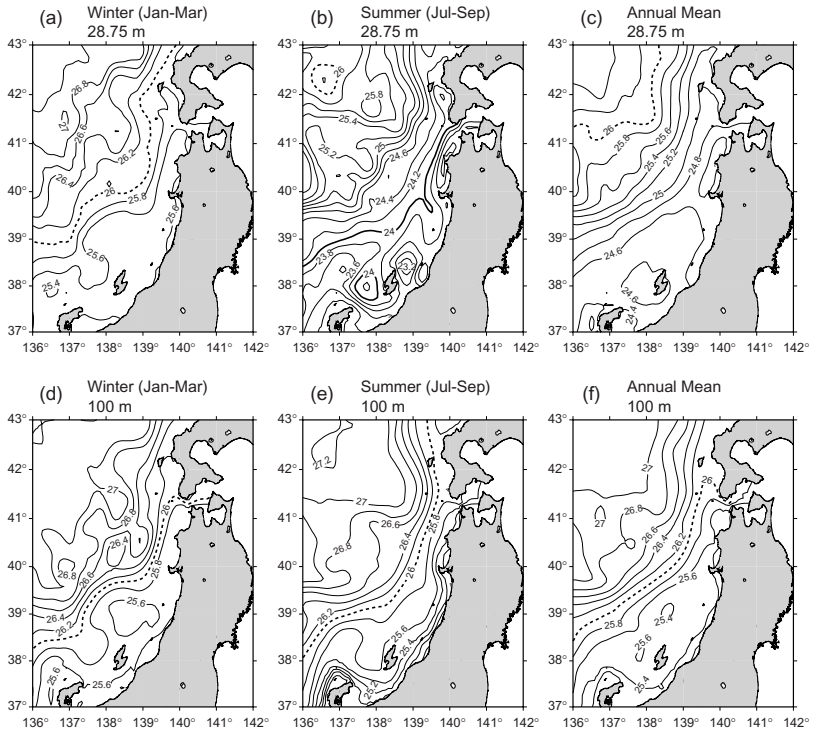

Fig. 16. Horizontal distribution of potential density (σ_θ) at depths of 28.75 and 100 m in winter (January–March), summer (July–September) and the annual mean field with C.I. = 0.2 kg/m^3 in experiment EXP3. The thick and dashed line indicate the isopycnal line of 24.0 and 26.0 kg/m^3, respectively.

formed in the offshore region, which is not very apparent in the nearshore region (not shown in the figure). These model results can be regarded as a demonstration of the conclusion drawn by Watanabe *et al*. (2006), that the properties of the coastal water mass in the surface and subsurface layer are modified north of the Oga Peninsula, combined with the offshore SBTWC and eastward current along the subarctic front with relatively low temperature and high salinity.

Watanabe *et al*. (2006) divided the TWC water into two parts: the upper portion of the TWC (UPTWC) water with high temperature, low salinity and potential density less than 24.0σ_θ, and the lower portion of the TWC (LPTWC) water with relatively low temperature, high salinity and potential density between 24.0 and 26.0σ_θ. Based on their definition of the UPTWC and the LPTWC, the volume transports of each density range across lines A–J are estimated in experiment EXP3 (Fig. 15). The magnitude is relatively good compared with the observational estimate and the directions also agree well with each other, apart from lines C2 and F. The northward volume transport of the UPTWC and the LPTWC increases at lines F and G (Figs. 15(b) and (c)), indicating that the SBTWC is combined with the FBTWC north of the Oga Peninsula. The northward volume transport of the denser water with potential density between 26.0 and 27.0σ_θ increases at line F in the observational results, while it increases at line G in experiment EXP3 (Fig. 15(d)). After the increase of northward volume transport of the UPTWC, the LPTWC and the denser water to the north of the Oga Peninsula, about half of the UPTWC and the LPTWC flows out through line H near the Tsugaru Strait, whereas the volume transport of the denser water is small (0.11 Sv) across line H in experiment EXP3. As a consequence, the denser water gradually comes to occupy a large amount of northward volume transport along the west coast of Hokkaido (lines I and J).

3.3 Seasonal variation of the branches of the TWC

The seasonal variation of the branches of the TWC in 2000 is examined in experiment EXP3, which can not be crystallized from the observation made in the restricted period of September and October by Watanabe *et al*. (2006). In order to discuss the seasonal variation, the definition of the UPTWC and the LPTWC explained above seems to be inadequate, because the water properties of the UPTWC change greatly throughout the year (Ogawa, 1983). Figure 16 displays the horizontal distribution of potential density at 28.75 m and 100 m depth, which is almost equivalent to the center depth of the UPTWC and

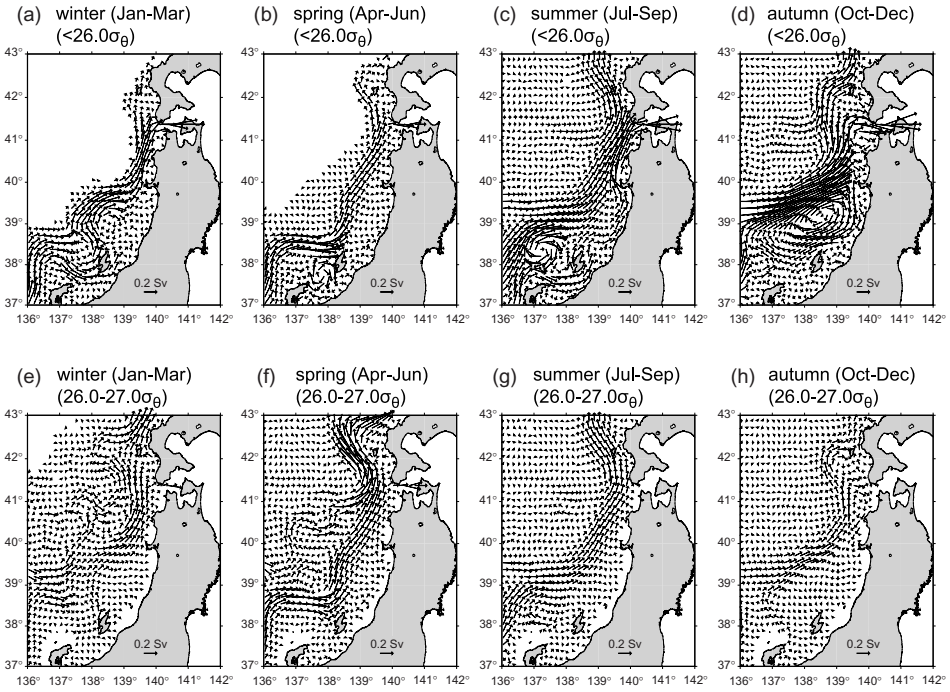

Fig. 17. Horizontal distribution of volume transport vector for the TWC water (<26.0σ_θ) and the denser water (26.0–27.0σ_θ) in winter (January–March), spring (April–June), summer (July–September) and autumn (October–December) in experiment EXP3. The volume transport vector is calculated in a cell and it is plotted at every 1/6° grid interval in both latitude and longitude. The white area indicates the region where no corresponding water mass exists.

the LPTWC, judging from Fig. 13. It is demonstrated that the water mass with potential density less than 24.0σ_θ occupies the depth of 28.75 m in the nearshore region in summer (Fig. 16(b)); on the other hand, it disappears in the eastern Japan Sea in winter (Fig. 16(a)). It is found that the potential density at 100 m depth is not very much changed near the northwestern Japanese coast throughout the year, ranging from 24.0 to 26.0σ_θ (Figs. 16(d), (e), and (f)). Hence, this study allows us plausibly to identify the water mass with potential density less than 26.0σ_θ hereafter as the TWC water, when discussing the seasonal variation of the TWC. In addition, the water mass with potential density between 26.0 and 27.0σ_θ is defined as the denser water to examine the structure below the TWC water.

Figure 17 displays the volume transport vector for the TWC water (<26.0σ_θ) and the denser water (26.0–27.0σ_θ) in winter, spring, summer and autumn. From the diagram for the TWC water, the coastal current along the northwestern Honshu Island comparable to the FBTWC is prominent in summer (July–September) (Fig. 17(c)), which is identical to the schematic flow pattern suggested by observation in September and October 2000 (figure 9 in Watanabe *et al.*, 2006). Although the FBTWC is continuous along the coast in their chart, the numerical experiment suggests that it degenerates along the coast south of the Oga Peninsula in other seasons, especially in the nearshore region between the Sado Strait and the Oga Peninsula. Even the southward countercurrent is found south of the Oga Peninsula in autumn by the large anticyclonic eddy to the north of Sado Island (Fig. 17(d)). Strong eddy activity north of Sado Island is also reflected in the relatively large standard deviation of sea surface height, of 15–20 cm in the satellite altimeter data (Fig. 2). As for the SBTWC, it flows northeastward with meanders and eddies in the offshore region deeper than 1000 m (Fig. 1) to the north of the Sado Island and it is combined with the coastal current north of the Oga Peninsula throughout the year (Figs. 17(a)–(d)). This northeastward flow pattern is equivalent to the current axis estimated from the largest long-term mean temperature gradients (figure 18 in Hase *et al.*, 1999), suggesting that the SBTWC is strongly steered by the bottom topography west of the Noto Peninsula, which flows along the continental shelf break through the quasi-geostrophic adjustment by topographic Rossby waves propagating along the shelf break. However, the mainstream of the SBTWC is not correlated with the shelf break east of the Noto Peninsula, since the shelf region is immature and narrow, suggesting that any propagation of topographic Rossby waves is interrupted. The SBTWC transforms from barotropic flow to baroclinic flow near the Noto Penin-

sula and as a consequence it separates from the continental shelf break flowing in the offshore region in the eastern Japan Sea (Nakada *et al*., 2002). The numerical experiment described in this study demonstrates that the SBTWC is not controlled by the bottom topography and it flows in the offshore region deeper than 1000 m in the eastern Japan Sea throughout the year. It is noted that the denser water as well as the TWC water is advected northeastward north of the Sado Island and eventually to the nearshore region of the northern Honshu Island throughout the year (Figs. 17(e)–(h)), which is identical to the schematic flow pattern given by Watanabe *et al*. (2006). In the Tsugaru Strait, the TWC water occupies most of the Tsugaru Warm Current flowing out to the Pacific Ocean in summer and autumn; on the other hand, the denser water continues to flow northward without entering the Tsugaru Strait, while it is apparent that part of the denser water flows out to the Pacific Ocean together with the TWC water in winter and spring, indicating the seasonal variability of the water mass in the Tsugaru Warm Current.

The seasonal variation of volume transport through the lines in the coastal region and schematic flow pattern is shown in Fig. 18 in experiment EXP3. It is suggested that the FBTWC is continuous along the coast east of the Noto Peninsula in summertime (July–September) with the volume transports of 0.50 Sv across the Sado Strait and 0.58 Sv south of the Oga Peninsula, respectively (Fig. 18(c)). The FBTWC water is modified north of the Oga Peninsula, mixing with the SBTWC water flowing in the offshore region and the volume transport of coastal current, then continues to increase along the northwestern coast of Honshu Island up to 1.40 Sv south of the Tsugaru Strait. It is noted that most of the modified water eventually flows out through the Tsugaru Strait with a volume transport of 1.34 Sv, while the residual current continues to flow northward along the west coast of Hokkaido. Although this residual current must itself be weak (0.06 Sv), the substantial volume transport of 0.97 Sv is investigated along the west coast of Hokkaido. This might be attributed to intensification by the eastward current established by the subarctic front intruding into the residual current near a southern tip of Hokkaido without entering the Tsugaru Strait in summertime. Close examination reveals that the denser water is not carried by the FBTWC but by the SBTWC and the eastward current along the subarctic front, and the throughflow transport is absent across the Tsugaru Strait in summertime, as shown in Fig. 18(d). In wintertime (January–March) it is suggested that the FBTWC degenerates between the Sado Strait and the Oga Peninsula (Fig. 18(a)). As for the SBTWC, it is pronounced in the offshore region deeper than 1000 m north of Sado Island, flowing northeastward in wintertime, suggesting that the mainstream of the SBTWC must persist

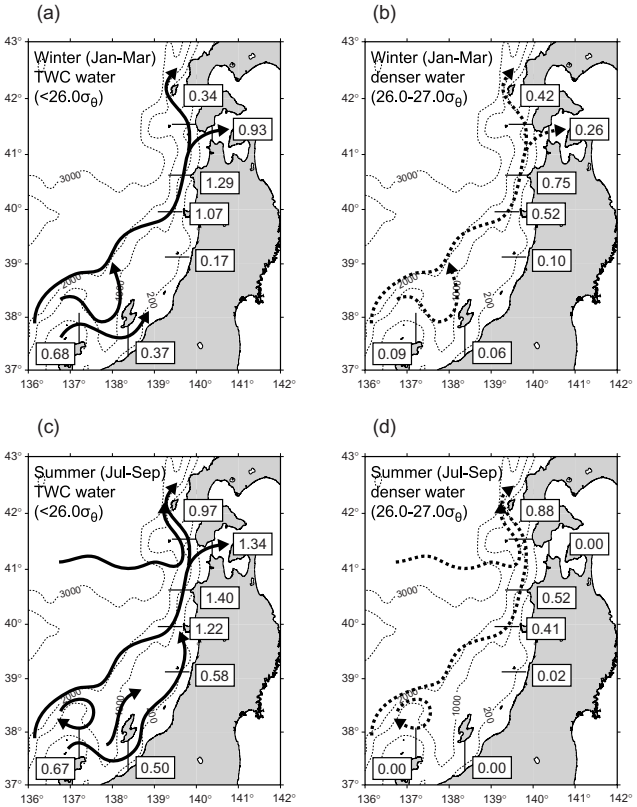

Fig. 18. Schematic current chart in winter (January–March) and summer (July–September) in the eastern Japan Sea in experiment EXP3. Solid and dashed lines indicate the TWC water (<26.0σ_θ) and the denser water (26.0–27.0σ_θ), respectively. Numbers denote the volume transports normal to each line in Sv where a positive value means eastward or northward direction.

there throughout the year in spite of the seasonal variation associated with meanders and eddies. From the standpoint of estimating the volume transport along northwestern Honshu Island and Hokkaido, a large amount of the TWC water along northwestern Honshu Island flows out as the Tsugaru Warm Current (0.93 Sv), while the remainder continues to flow northward along the west coast of Hokkaido in wintertime, which is the same as the feature in summertime. The different phenomena between wintertime and summertime relate to the intrusion of the eastward current along the subarctic front into the nearshore region along the west coast of Hokkaido, which is hardly found in wintertime. Moreover, the denser water is carried to the Pacific Ocean through the Tsugaru Strait (0.26 Sv) along with the TWC water in wintertime (Fig. 18(b)).

4. Conclusions

Numerical experiments have been performed to reproduce the branches of the TWC in the eastern Japan

Sea using the volume transports obtained by ADCP measurements through the Tsushima Straits and the Tsugaru Strait as the inflow and outflow boundary conditions. Although the sea level variation along the southwestern Japanese coast is effectively reproduced in the case without any data assimilation, there are some mismatches of the current structure as well as the sea level variation in the nearshore region to the east of the Noto Peninsula. In this study, the effect of data assimilation on current structure in the nearshore region is surveyed using the satellite altimeter data and the sea level data at 19 tide-stations along the Japanese coast. As a consequence, it was found that the assimilation of only satellite altimeter data may not be enough to improve the current structure near the coast on account of inaccuracy in the satellite altimeter data in the shallow region, although an improvement in the ocean interior has been demonstrated by many data assimilation experiments (Hirose *et al*., 2007). The data assimilation experiment using sea level variation obtained by the coastal tide-stations as well as the satellite altimeters basically reproduces the current structure reported by Watanabe *et al*. (2006). The improvement of current structure by the data assimilation of sea level variation at the coastal tide-stations is outstanding, especially in the northern Japan Sea, which must be accomplished through the quasi-geostrophic adjustment by sea level difference between the satellite altimeters and the coastal tide-stations.

The seasonal variation of the branches of the TWC in the eastern Japan Sea in 2000 is studied in the data assimilation experiment using sea level variation obtained by the satellite altimeters and the coastal tide-stations. The schematic flow pattern of the TWC water ($<26.0\sigma_\theta$) and the denser water (26.0–$27.0\sigma_\theta$) below the TWC water in summertime (July–September) is comparatively consistent with a distinct feature suggested by the ADCP and CTD measurement in September and October 2000. The data assimilation experiment suggests that the FBTWC is continuous along the coast east of the Noto Peninsula and the FBTWC water is modified north of the Oga Peninsula mixing with the offshore SBTWC water in summertime. It is also suggested that a large amount of the modified water flows out through the Tsugaru Strait, while the residual current flows toward the north along the west coast of Hokkaido strengthened by the intrusion of the eastward current along the subarctic front. In wintertime (January–March), it is found that the FBTWC degenerates between the Sado Strait and the Oga Peninsula, and the SBTWC is conspicuous in the offshore region deeper than 1000 m north of the Sado Island flowing northeastward as well as in summertime suggesting that the mainstream of the SBTWC persists there throughout the year. The different phenomenon between in wintertime and in summertime is that the eastward current along the subarctic front hardly intrudes into the nearshore region along the west coast of Hokkaido in wintertime. In addition, the throughflow transport of the denser water occurs across the Tsugaru Strait only in wintertime.

It should be noted that the branches of the TWC exhibit year-on-year variation and it is expected that the present study will provide a useful contribution to any future understanding of the characteristic of the TWC. It is of great importance to reproduce the branches of the TWC with the view of assessing the movement of pollutants in the ocean such as an oil spill incident involving the Russian tanker "*Nakhodka*" in early January 1997. A system for assessing the marine environment in the Japan Sea with RIAMOM and a particle random-walk model is currently under development at Japan Atomic Energy Agency (JAEA). In the future, the system will progress further thanks to collaboration with the Research Institute for Applied Mechanics (RIAM), Kyushu University.

Acknowledgements

The authors express their sincere thanks to the captain and the crew of the ferryboat "*Camellia*" and the staff of the Camellia Line, Ltd. We would like to extend our gratitude to the HIGASHINIHON-FERRY Co., Ltd., the captain and the crew of "*M.V. Virgo*" for their cooperation. Appreciation is also extended to the editor and two anonymous reviewers for their constructive comments. Satellite altimeter data were provided by the Physical Oceanography Distributed Active Archive Center (PO-DAAC) at Jet Propulsion Laboratory (JPL), National Aeronautics and Space Administration (NASA). Sea level data at the coastal tide-stations were obtained from the Japan Oceanographic Data Center (JODC). Numerical experiments were conducted on SGI Altix3700 Bx2 at the Center for Computational Science and e-Systems (CCSE), Japan Atomic Energy Agency (JAEA). This study was performed under a framework of collaboration between Kyushu University and JAEA.

References

Adcroft, A., C. Hill and J. Marshall (1997): Representation of topography by shaved cells in a height coordinate ocean model. *Mon. Wea. Rev*., **125**, 2293–2315.

Blumberg, A. F. and G. L. Mellor (1987): A description of a three-dimensional coastal ocean circulation model. p. 1–16. In *Three-Dimensional Coastal Ocean Models*, ed. by N. S. Heaps, American Geophys. Union, Washington, D.C.

Fu, L.-L., I. Fukumori and R. N. Miller (1993): Fitting dynamic models to the Geosat sea level observations in the Tropical Pacific Ocean. Part II, A linear wind-driven model. *J. Phys. Oceanogr*., **23**, 2162–2181.

Fukumori, I. and P. Malanotte-Rizzoli (1995): An approximate Kalman filter for ocean data assimilation: An example with an idealized Gulf Stream model. *J. Geophys. Res*., **100**, 6777–6793.

Gent, P. R. and J. C. McWilliams (1990): Isopycnal mixing in ocean circulation models. *J. Phys. Oceanogr.*, **20**, 150–155.
Gill, A. E. (1982): *Atmosphere-Ocean Dynamics*. Academic Press, San Diego, Calif., 662 pp.
Haney, R. L. (1971): Surface thermal boundary conditions for ocean circulation models. *J. Phys. Oceanogr.*, **1**, 241–248.
Hase, H., J.-H. Yoon and W. Koterayama (1999): The current structure of the Tsushima Warm Current along the Japanese coast. *J. Oceanogr.*, **55**, 217–235.
Hirose, N. (1999): Assimilation of satellite altimeter data with circulation models of the Japan Sea. Ph.D. Thesis, Kyushu Univ., 120 pp.
Hirose, N., H. Kawamura, H.-J. Lee and J.-H. Yoon (2007): Sequential forecasting of the surface and subsurface conditions in the Japan Sea. *J. Oceanogr.*, **63**, 467–481.
Ishikawa, K., Y. Isoda and T. Aiki (2007): Seasonal variation in the Nearshore Branch of the Tsushima Warm Current as inferred from coastal sea level data. *Oceanography in Japan*, **16**, 223–236 (in Japanese with English abstract).
Ito, T., O. Togawa, M. Ohnishi, Y. Isoda, T. Nakayama, S. Shima, H. Kuroda, M. Iwahashi and C. Sato (2003): Variation of velocity and volume transport of the Tsugaru Warm Current in the winter of 1999–2000. *Geophys. Res. Lett.*, **30**(13), 1678, doi:10.1029/2003GL017522.
Katoh, O. (1994): Structure of the Tsushima Current in the southwestern Japan Sea. *J. Oceanogr.*, **50**, 317–338.
Katoh, O., K. Morinaga, K. Miyaji and K. Teshima (1996): Branching and joining of the Tsushima Current around the Oki Islands. *J. Oceanogr.*, **52**, 747–761.
Lee, H.-C. (1996): A numerical simulation for the water masses and circulations of the Yellow Sea and the East China Sea. Ph.D. Thesis, Kyushu Univ., 150 pp.
Lee, H.-J., J.-H. Yoon, H. Kawamura and H.-W. Kang (2003): Comparison of RIAMOM and MOM in modeling the East Sea/Japan Sea circulation. *Ocean Polar Res.*, **25**, 287–302.
Naganuma, K. (1977): The oceanographic fluctuations in the Japan Sea. *Mar. Sci.* (*Kaiyo Kagaku*), **9**, 137–141 (in Japanese with English abstract).
Nakada, S., Y. Isoda and K. Kusahara (2002): Response of the coastal branch flow to alongshore variation in shelf topography off Toyama Bay. *Oceanography in Japan*, **11**, 243–258 (in Japanese with English abstract).
Noh, Y. and H.-J. Kim (1999): Simulations of temperature and turbulence structure of the oceanic boundary layer with the improved near-surface process. *J. Geophys. Res.*, **104**, 15621–15634.
Ogawa, Y. (1983): Seasonal changes in temperature and salinity of water flowing into the Japan Sea through the Tsushima Strait. *Bull. Jpn. Soc. Fish. Oceanogr.*, **43**, 1–8 (in Japanese with English abstract).
Sakaida, F., J. Kudoh and H. Kawamura (2000): A-HIGHERS—The system to produce the high spatial resolution sea surface temperature maps of the Western North Pacific using the AVHRR/NOAA. *J. Oceanogr.*, **56**, 707–716.
Sasajima, Y., S. Nakada, N. Hirose and J.-H. Yoon (2007): Structure of the subsurface counter current beneath the Tsushima Warm Current simulated by an ocean general circulation model. *J. Oceanogr.*, **63**, 913–926.
Shuman, F. G. (1957): Numerical methods in weather prediction: II. Smoothing and filtering. *Mon. Wea. Rev.*, **85**, 357–361.
Takikawa, T., J.-H. Yoon and K.-D. Cho (2005): The Tsushima Warm Current through Tsushima Straits estimated from ferryboat ADCP data. *J. Phys. Oceanogr.*, **35**, 1154–1168.
Toba, Y., K. Tomizawa, Y. Kurasawa and K. Hanawa (1982): Seasonal and year-to-year variability of the Tsushima-Tsugaru Warm Current system with its possible cause. *La Mer*, **20**, 41–51.
Tsujino, H., H. Nakano and T. Motoi (2008): Mechanism of currents through the straits of the Japan Sea: Mean state and seasonal variation. *J. Oceanogr.*, **64**, 141–161.
Watanabe, T., O. Katoh and H. Yamada (2006): Structure of the Tsushima Warm Current in the northeastern Japan Sea. *J. Oceanogr.*, **62**, 527–538.
Webb, D. J., B. A. de Cuevas and C. S. Richmond (1998): Improved advection schemes for ocean models. *J. Atmos. Oceanic Technol.*, **15**, 1171–1187.
Yarichin, V. G. (1980): Study state of the Japan Sea circulation. p. 46–61. In *Problems of Oceanography*, ed. by V. Pokudov, Hydrometeoizdat, Leningrad (in Russian).
Yoon, J.-H. (1982): Numerical experiment on the circulation in the Japan Sea, Part III. Mechanism of the nearshore branch of the Tsushima Current. *J. Oceanogr. Soc. Japan*, **38**, 125–130.
Yoon, J.-H. (1991): The branching of the Tsushima Current. *Rep. Res. Inst. Appl. Mech. Kyushu Univ.*, **38**, 1–21.